Lagrangian and Eulerian modelling of 106Ru atmospheric transport in 2017 over northern hemisphere

Léo Adenis, Sylvain Mailler, Laurent Menut, Pascal Achim, Sylvia Generoso

Journal of Environmental Radioactivity 275 (2024) 107416

Contents lists available at ScienceDirect

Journal of Environmental Radioactivity

journal homepage: www.elsevier.com/locate/jenvrad

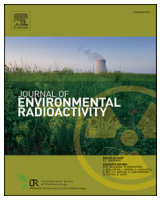

Lagrangian and Eulerian modelling of ^{106}Ru atmospheric transport in 2017 over northern hemisphere

Léo Adenis *, Sylvain Mailler, Laurent Menut, Pascal Achim, Sylvia Generoso

ARTICLE INFO

Dataset link: https://www.lmd.polytechnique.fr

Dataset link: https://doi.org/10.14768/8afd9058-909c-4827-94b8-69f05f7bb46d

Dataset link: https://www.flexpart.eu/downloads

Keywords:
Atmospheric transport
Modelling
Eulerian model
CHIMERE
Lagrangian model
FLEXPART

ABSTRACT

In September 2017, numerous measurement stations recorded large surface concentrations of ^{106}Ru in Europe. This event was well recorded by various monitoring stations worldwide and offer a valuable framework to compare the modelling strategies deployed to quickly evaluate where the plume goes and with what concentrations. In general, the source and its intensity are not known and hypotheses have to be done. Models have to be fast and accurate: Lagrangian and Eulerian are often used but rarely compared. In this study, the FLEXPART Lagrangian model and the WRF-CHIMERE Eulerian models are used to simulate the emissions, transport and deposition of this source of ^{106}Ru. First, it is shown that the hypothesis of location, timing and intensity of the source is realistic, by comparison to surface measurements. Second, sensitivity analysis performed with the Eulerian model and several transport scheme showed that this model may provide better results than the Lagrangian one. It opens the door to further development, including chemistry and mixing with other pollutants during these specific events.

1. Introduction

In September and October 2017 a plume containing ruthenium 106 (^{106}Ru) was detected by several radioactivity monitoring networks across the Northern hemisphere. ^{106}Ru is a fission product of specific industrial or military nuclear processes, has no natural sources and a half-life of 371.5 days. Therefore, any atmospheric detection of ^{106}Ru necessarily traces back to an anthropogenic release. Since the detonation of nuclear weapons is one of the possible sources of ^{106}Ru in the atmosphere, this isotope is monitored on a daily basis by the Comprehensive Nuclear-Test-Ban Treaty Organization (CTBTO) International Monitoring System (IMS) all over the globe. During the 2017 event of ^{106}Ru, this isotope has been detected in stations from the IMS and from the “Ring of 5” (Ro5). The Ro5 is an informal association of scientists mainly in Europe. It exists since 1983 with the purpose of exchanging information on unusual concentrations of radionuclides in the atmosphere. It is composed of 110 sites of aerosols collection in Europe. The first alert signal from the Ro5 network came on the 2nd of October from an Italian station. On the same day another station, this time in Czech Republic, showed sign of ^{106}Ru activity. The following two days numerous stations in Europe detected ^{106}Ru (Greece, Sweden, Austria, Poland). Several days after, detections occurred outside of Europe. The first detections on the IMS occurred on the 1st of October at the Swedish station (SE63). In the East ^{106}Ru was detected on the far end of Russia and in Mongolia between the 8th and the 13th of October. On the West side the pollution arrived and was measured in the IMS stations situated in Guadeloupe and in Florida respectively on 18th and on the 21st of October. Activity concentrations in Europe were ranging from tenths of $\mu Bq.m^{-3}$ up to a maximum of 176 ± 18 $mBq.m^{-3}$ in Romania. Activity concentrations on the later detections were of the order of tens of $\mu Bq.m^{-3}$ in both east and west directions. Most of these measurements have been compiled in Masson et al. (2019). Substantial events of atmospheric release of ^{106}Ru are extremely rare, so that the most likely scenario is that all these detections have been a consequence of one single event of ^{106}Ru release in the atmosphere.

Apart from presenting and analyzing the available measurements, some studies published so far on this event include scenarii regarding the localization, time, duration and magnitude of the ^{106}Ru release (Masson et al., 2019; Saunier et al., 2019; Sørensen, 2018; Dumont Le Brazidec et al., 2020, 2021; Western et al., 2020).

In Dumont Le Brazidec et al. (2020) the Eulerian model ldX for atmospheric transport of IRSN’s operational platform (Tombette et al.,

* Corresponding author.
E-mail addresses: leo.adenis@lmd.ipsl.fr, leo.adenis@outlook.fr (L. Adenis).

https://doi.org/10.1016/j.jenvrad.2024.107416
Received 29 November 2023; Received in revised form 13 March 2024; Accepted 13 March 2024
Available online 23 March 2024

Table 1
Few scenarii to describe the causes of the ^{106}Ru pollution of 2017.

Reference	Emission Time	Location	Activity
Dumont Le Brazidec et al. (2021)	09/25/2017	[59° : 61°]E, [55° : 66°]N	[200 : 450] TBq
Sørensen (2018)	0–16UTC 09/27/2017	NIIAR nuclear facility	460 TBq
Sørensen (2018)	5–13UTC 09/25/2017	Mayak Production Association	1100 TBq
Saunier et al. (2019)	12–18UTC 09/26/2017	Mayak Production Association	∼ 250 TBq
Western et al. (2020)	12–18UTC 09/24/2017	Mayak Production Association	441 ± 13 TBq
Scenario of this paper	18–19UTC 09/24/2017	Mayak Production Association	500 TBq

2014) is used in conjunction of a Markov Chain Monte Carlo (MCMC) method to adjust the origin of emission and its amplitude for the transport model so that it yields results in agreement with the measurements. Meteorology from two sources were used: European Centre for Medium-Range Weather Forecasts (ECMWF) reanalysis of global weather (ERA5 HRES) (Hersbach, 2019) and Météo France reanalysis with ARPEGE model (Pailleux et al., 2000). Saunier et al. (2019) presents also results using the Eulerian model ldX but use inverse modelling to reconstruct the source term and origin. Meteorology from ARPEGE by Météo France has been used. In Western et al. (2020) a Lagrangian atmospheric transport model is used, the Numerical Atmospheric-dispersion Modelling environment (NAME, Jones et al. (2007)) from UK Met Office also with a MCMC approach for the source estimation. This Lagrangian model were driven by numerical weather prediction data from Met Office Unified Model (Walters et al., 2014). Even though these publications vary between each other due to their different working hypotheses, meteorology sources and methodologies, all of them are consistent with a release of ^{106}Ru some time between Sept. 24 and Sept. 27 somewhere in western Russia, in the order of hundreds of TBq.

In such events of atmospheric release of isotopes of interest, numerical modelling has two main purposes (or other pollutants released by natural or accidental events). Firstly, as discussed above, numerical models can help construct and test emission scenarii that can explain the detected pollution. Secondly, once a scenario is proposed (through inverse modelling or as a hypothesis), numerical models can be used as forecast tools to estimate in advance the location, shape and concentration of the plume, which is in turn useful to permit adequate reaction and planning depending on the type of event (*e.g.* flight restrictions in case of volcanic ash release, Plu et al. (2021)). Two types of model are usually used to describe atmospheric transport of pollutants: Lagrangian and Eulerian models. While Lagrangian models follow air parcels and the pollutants they contain along their atmospheric motion (Brunner (2012)), Eulerian models divide the space into elementary volumes (grid cells), and represent the evolution of the concentrations of pollutants within each of the grid cell. Most chemistry-transport models – *e.g.* Geos-Chem – are designed with an Eulerian approach (Henne et al., 2013). Compared to Lagrangian models, Eulerian models tend to present a numerical diffusion that can deteriorate their precision (Eastham and Jacob, 2016; Zhuang et al., 2018). Eulerian models contain different possible transport schemes with different orders of accuracy leading to higher or lower numerical diffusion.

In this study we will propose a scenario to describe this event, confirm it with our simulations. At the same time we will compare, with said scenario of emission an Eulerian model, CHIMERE, and a Lagrangian model, FLEXPART. This comparison aims to identify if CHIMERE is suffering from the numerical diffusion known for Eulerian models and in case of an operative work can CHIMERE, without taking in account potential benefits of an Eulerian model yet (advanced chemistry and radioactive decay chains for example), be competitive compared to FLEXPART.

Section 2 describes the tools used in this study, observations in section 2.1, modelling in Section 2.2 and methods in Section 2.3. Results of simulations and comparisons to observations are discussed in Section 3 and conclusions and perspectives are discussed in section 4.

2. Observations and models

2.1. Observations

As this event is a very rare occurrence, the last documented detection at the globe's scale of ^{106}Ru dates of Chernobyl accident (Paatero et al., 2007), a lot of work has been done to pinpoint the origin of the emission and its intensity using the measurements done all over Europe. Table 1 sums up the scenarii proposed in Masson et al. (2019); Saunier et al. (2019); Sørensen (2018); Dumont Le Brazidec et al. (2021); Western et al. (2020) and the one we have chosen.

In Masson et al. (2019) a large number of measurements over many locations over Europe were compiled. They are mostly composed of measurements done and exchanged in the context of the Ro5. We added measurements from a few stations of the IMS from the CTBTO. Those will be used to compare the models with each others and their respective efficiency to reproduce reality. In total we have 1340 measurements over 337 stations available. Fig. 1 is map of all the stations with available measurements. All measurements were done with various thresholds of detection (from 0.1 $\mu Bq.m^{-3}$ to 10 $\mu Bq.m^{-3}$) and various sampling frequency: daily for the IMS stations, up to a few days in Ro5 stations. A larger sampling time will mean that measurement will be more representative of the average of the activity concentration and will be less accurate to detect peaks of shorter duration.

In section 2.3 we will define a detection threshold for our simulation and a condition to determine if simulations are in agreement with each measurement. Comparisons between model and measurements will be presented in section 3.3.

2.2. Models

Two atmospheric transport models are part of our study: an Eulerian model, CHIMERE and a Lagrangian model FLEXPART.

We used CHIMERE v2020r3 (Menut et al., 2021) an Eulerian chemistry-transport model (CTM) using WRF meteorological files as input. Multiple advection schemes are available in CHIMERE for both horizontal and vertical transports. Flux-form, upwind-biased advection schemes are the most common way to treat the advection problem in Eulerian chemistry-transport models. These schemes, based on the ideas of Godunov (1959), treat advection by estimating the mass fluxes between neighboring cell based on reconstructed estimates of tracer mixing ratio in the upwind cell. This reconstruction can be uniform as in the Godunov (1959) advection scheme (often known as donor-cell scheme, van Leer (2003)), linear as in the Van Leer (1977) and the Walcek (2000) schemes, or parabolic as in the Piecewise Parabolic Method (PPM) of Colella and Woodward (1984). A combination of the PPM and the Walcek schemes, named PPM+W for "Piecewise Parabolic Method + Walcek", has been designed and proven more accurate than both the PPM and Walcek schemes in a bidimensional academic framework with active chemistry (Mailler et al., 2023b). The Després and Lagoutière (1999) scheme is a antidiffusive advection scheme which has been implemented in the CHIMERE chemistry-transport model and proven to reduce plume diffusion at least for volcanic plumes in the free troposphere (Mailler et al., 2021; Lachatre et al., 2020, 2022). All the above-mentioned schemes are monotonous and conserve mass, which are two desirable properties for advection in chemistry-transport

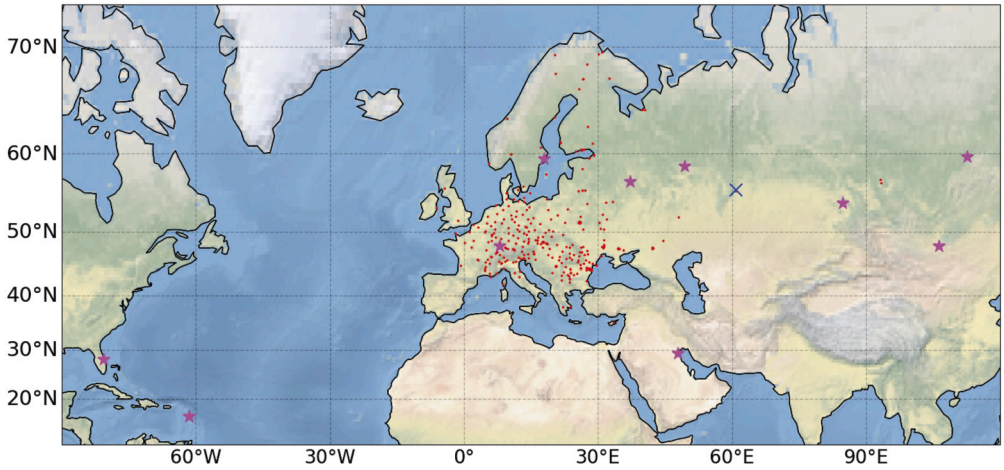

Fig. 1. Positions of all measurements stations in the northern hemisphere that have detected ^{106}Ru during this event. Red dots represent the Ro5 stations and the magenta stars the IMS stations. The proposed location of the emission source is marked by a blue cross at 55.70° N, 60.76° E. (For interpretation of the colors in the figure(s), the reader is referred to the web version of this article.)

Table 2
Advection schemes used in our simulation using CHIMERE.

Simulation Label	Horizontal advection	Vertical advection
VLVL	Van Leer (Van Leer, 1977)	Van Leer (Van Leer, 1977)
VL	Van Leer (Van Leer, 1977)	Deprés-Lagoutière (Després and Lagoutière, 1999)
PPM	Piecewise Parabolic Method (Colella and Woodward, 1984)	Deprès-Lagoutiére (Després and Lagoutière, 1999)
W	Walcek (Walcek, 2000)	Deprés-Lagoutière (Després and Lagoutière, 1999)
PPMW	PPM+W (Mailler et al., 2023b)	Deprés-Lagoutière (Després and Lagoutière, 1999)

models. While these schemes are not the only ones used in chemistry-transport models, their use is quite frequent. The CHIMERE model implements the Van Leer, Walcek and PPM schemes in the horizontal direction and the Van Leer and Després and Lagoutière (1999) schemes in the vertical direction (Menut et al., 2021). The Walcek (2000) scheme is also implemented in CCATT-BRAMS (Freitas et al., 2012) and LOTOS-EUROS (Timmermans et al., 2022). The PPM scheme, apart from the CHIMERE model, is also implemented in the advection framework of the Geos-CHEM chemistry-transport model (Martin et al., 2022), and in the CMAQ chemistry-transport model (Byun and Schere, 2006; Zhao et al., 2020)).

As described in Menut et al. (2021), CHIMEREv2020r3 includes the schemes of Van Leer (1977) – hereinafter "Van Leer scheme" –, Walcek (2000) – hereinafter "Walcek scheme" – and Colella and Woodward (1984) – hereinafter "PPM scheme" – for horizontal advection. In the vertical direction, the advection schemes implemented in CHIMEREv2020r3 are the Van Leer scheme and the Després and Lagoutière (1999) scheme – hereinafter, "DL99 scheme" –. While the Van Leer, Walcek and PPM schemes are classical in chemistry-transport models, the DL99 is not. It has been shown recently (Mailler et al., 2021; Lachatre et al., 2020, 2022) that the use of this antidiffusive advection scheme in chemistry-transport models permits to reduce numerical diffusion in both academic and real cases. To our knowledge, CHIMERE is the only chemistry-transport model implementing this scheme. Apart from these schemes, the version of CHIMERE we have used for the present study includes the PPM+W advection scheme. The PPM+W scheme, standing for "Piecewise Parabolic Method + Walcek" is a third-order advection scheme based on the PPM and Walcek schemes. In zones of monotonous gradient, the PPM+W scheme is identical to the PPM scheme, with a parabolic reconstruction of the mixing ratio in each cell. However, in the cells neighboring a mixing-ratio extremum, the PPM+W scheme performs a linear (and not parabolic) reconstruction of the mixing ratio inside the cell. This reconstruction, following the flux adjustments of Walcek (2000), permits to reduce the excess of diffusion in the vicinity of the maxima. Mailler et al. (2023b) has shown that the PPM+W advection scheme performs better than both PPM and Walcek in a 2d, academic testcase with active chemistry. Since Mailler et al. (2023b) have worked in a purely academic 2d framework with a toy chemistry-transport model (ToyCTM v1, Mailler and Pennel (2023)), the present study presents the first implementation and use of this advection scheme in a full-fledge chemistry-transport model on an applied real uncontrolled pollution case.

We have tested various model configurations in terms of advection schemes to check their impact on numerical diffusion and model performance. Table 2 summarizes all the combinations of advection schemes we tested with CHIMERE and their associated references. The simulation domain covers the entire Northern hemisphere with resolution $\delta x \simeq 100$ km, a coarse resolution adapted to the scale of this event. This domain has been built with a North polar stereographic projection. 30 vertical levels from the surface to 300 hPa (approximately up to 9.8 km of altitude) have been used. Deposition of particles on the surface is represented using the Zhang et al. (2001) parameterization. Meteorology has been simulated with the WRF-ARW model version 3.7.1 (Skamarock et al., 2008). The WRF simulations have been performed on the same grid as CHIMERE using the WRF-CHIMERE simulation framework (Briant et al., 2017). The WRF simulation has been forced at the boundaries and driven within the simulation domain by analyses from the Global Forecast System (GFS) provided by the US National Centers for Environmental Prediction (NCEP). Nudging towards the GFS analyses inside the simulation domain has been performed using spectral nudging (von Storch et al., 2000). Both CHIMERE and WRF are using the same domain. As described in Briant et al. (2017), in the WRF-CHIMERE simulation framework, the meteorological fields are updated in CHIMERE at a high frequency. For this study, these fields are provided by WRF to CHIMERE every 20 minutes. Two options are available in CHIMERE for the WRF simulations: either WRF is running as the same time as the CHIMERE simulation or WRF can be run on its own, the results saved and can be used multiple times as input in CHIMERE. We went with the later as we ran multiple numerical transportation schemes in CHIMERE.

Table 3
Main parameters for our simulations.

Parameter	CHIMERE	FLEXPART
Output Time Step	1 hour	1 hour
Time Step	20 minutes	10 minutes
Date of emission	18 UTC 09/24/2017	18 UTC 09/24/2017
Emission duration	1 hour	1 hour
Emission height	[10 : 20] m	[10 : 20] m
Dry Deposition scheme	Zhang et al. (2001)	Stohl et al. (2010)
In-cloud scavenging	Wang et al. (2014)	Hertel et al. (1995)
Below-cloud scavenging	Willis and Tattelman (1989)	McMahon and Denison (1979)
Number of height level	30	30
Number of particles	NA	5.10^6
Particle mean diameter	1.9 μm	1.9 μm
Particle diameter distribution sigma	0.3	0.3
Particle volumic mass	2.5×10^3 kg.m^{-3}	2.5×10^3 kg.m^{-3}
Horizontal Transport	VL, PPM, PPMW, W	Zero acceleration (Stohl et al., 2010)
Vertical Transport	VL, DPL	Zero acceleration (Stohl et al., 2010)
Meteo	WRF (with GFS 1° resolution as input and constraint)	GFS at 1° resolution
Simulation domain	Northern hemisphere for both models	

We used FLEXPART (v9.0.2) for our Lagrangian simulation. This version of FLEXPART is using GFS meteorological files as input (Stohl et al., 2010). We used 5.10^6 particles in our simulation. The output grid used in FLEXPART is defined as 260 per 260 cells with a resolution of 1.3846° for longitude and 0.423° for latitude on horizontal level and 30 height levels from surface to 9780 m corresponding to the highest level in CHIMERE domain. The output grid was chosen to be of the same resolution as in CHIMERE.

The meteorological files used in our FLEXPART simulations are the same GFS files with a 1° resolution used as input and constraining WRF when calculating the meteorological files used in CHIMERE (National Centers for Environmental Prediction, 2000).

In both FLEXPART and CHIMERE, we have used an inert aerosol tracer, disabling chemistry in CHIMERE and all decay in FLEXPART. The only mechanism to decrease the tracer quantity in these simulations is deposition. Particle tracer was emitted between 18h00 and 19h00 on the 24th of September 2017 at constant flux between 10 m and 20 m above ground at 55.70° N, 60.76° E.

Dry deposition is a very sensitive parameter when dealing with the life cycle of atmospheric aerosols, with very sharp variations of the dry deposition velocity as a function of diameter (Zhang et al., 2001). Even though Masson et al. (2019) has suggested a diameter inferior to 1 μm, this parameter is poorly constrained for our study case. With a typically quadratic dependence of the sedimentation speed of the particles relative to diameter in the Stokes regime (e.g. Mailler et al. (2023a)), the effect of a slightly different hypothesis on diameter over weeks of atmospheric advection of ^{106}Ru can dramatically affect the simulation results. Apart from the uncertainty on particle diameter, their shape is also unknown, which is also problematic since the shape of atmospheric aerosols strongly affects their settling speed (Mallios et al., 2020, 2021). In the present study, we have considered all the particles carrying ^{106}Ru to be spherical with density $\rho = 2500$ kg m^{-3} corresponding to typical mineral dust characteristic. The same unimodal size distribution for aerosols has been used for CHIMERE and FLEXPART (Table 3) in order to be able to compare both simulations.

To determine this common size distribution, several hypotheses for the log-normal distribution of aerosols have been tested in FLEXPART, and we have retained the hypothesis fitting best the observed results for the two most distant stations having detected this event (stations FRP28 in Guadeloupe and USP72 in Florida). This has led us to determine a mass-median diameter $D = 1.9$ μm for the particles, with a standard deviation $\sigma = 0.3$. Diameters much below this value would lead to largely overestimated activity concentrations at these stations, and conversely, diameters much larger would lead to underestimation. In order to better characterize the atmospheric transport of this and other events of aerosol advection in the atmosphere, a good knowledge of the size distribution, shape and density of the particles is needed, which not within our reach for the present study.

The main parameters of the CHIMERE and FLEXPART simulations are summarized in Table 3.

2.3. Metrics and statistical methods

This section will detail the tools we used in this paper to evaluate the performances of our simulations. First how we quantified and compared the diffusion of CHIMERE advections schemes with each other and with FLEPXART. And secondly how the comparison with measurements was done and how we evaluated the performances of our simulations.

To quantify plume diffusion, we will use the notion of half-volume, as introduced by Lachatre et al. (2020). These authors have introduced the half-volume as the smallest atmospheric volume that contains at least half the mass of tracer (in our case, ^{106}Ru). In our case, at the instant when the tracer is first released from its point source, the half-volume in the Eulerian simulation is the volume of the single model grid cell containing all the ^{106}Ru. As the plume is transported and diffused by winds and mixing fluxes, the half-volume will typically increase as the plume spreads in the atmosphere. This spread depends strongly on the diffusivity of the numerical schemes, with the less diffusive schemes leading to a smaller half-volume (Lachatre et al., 2020, 2022; Mailler et al., 2023b). For FLEPXART simulation, half-volume will be calculated with the projected output and so is defined exactly as for CHIMERE simulations. In this study the half-volume serves as a indicator of how much numerical diffusion occurs and not as an overall performance indicator for our simulations.

In a second part we will use the formalism of confusion matrices (*e.g.* Fawcett (2006)) to compare our model outputs with the available observations in terms of detection/non detection. This approach is commonly used for the prevision of “dichotomous weather events” (Stephenson, 2000). This approach will permit a quantitative comparison of the agreement of all the tested model configurations with ^{106}Ru detections at measurement stations. Those matrices are composed of four values and are defined as:

- True Positive (TP): ^{106}Ru was detected in both the simulation and measurements.
- True Negative (TN): ^{106}Ru was NOT detected in both the simulation and measurements.
- False Positive (FP): ^{106}Ru was detected in the simulation but NOT in measurements.
- False Negative (FN): ^{106}Ru was NOT detected in the simulation bust was in measurements.

Table 4
Example of confusion matrix between a simulation (SIM) and Measurements.

		Measured	
		Yes	No
SIM	Yes	TP	FP
	No	FN	TN

Table 5
Confusion matrix of Random no-skill model (RNS) for the ^{106}Ru pollution of 2017.

		Measured	
		Yes	No
RNS	Yes	207.3	319.7
	No	319.7	493.3

A theoretical example of confusion matrix is presented in Table 4. To compute all four values for our simulations, it is necessary to extract a single value in our simulations: positive (concentration is significant) or negative (concentration is not significant). The difficulty was to have a common framework to compare model and observations: measurements are located in a single location and are temporally integrated over different durations depending on the station and the measurement period. But they are already classified in an over (positive) or under (negative) a limit of detection. On the other hand, model concentrations are a mean value representative of a grid cell for one hour. To have the corresponding positive/negative value within our simulations, we went with the following: if the surface concentration (lowest level in the output grid) value is above a threshold during at least 1 hour over the period of the real measurement, the model scores are 'positive' and 'negative' otherwise. We chose a value of 10 µBq.m^{-3} for that threshold, corresponding to a low but realistic value of a plume passing over the station for a few hours. In total we have 1340 measurements covering two third of the simulated period with 514 being positive.

Once the confusion matrices are built, we computed eight indicators to summarize the performances of our models. We also compared their performances with a "random no-skill" model as defined by Stephenson (2000). This model is giving a random prediction for each event, respecting the same overall detection probability observed in measurements. The confusion matrix of the random no-skill model is presented in Table 5.

The statistical indicators we will use in the rest of our study are the following:

- Sensitivity $= TP/(TP+FN)$: quantifying the ability of the models to detect True Positive values. Sensitivity is also is called "Hit rate" in Stephenson (2000);
- Specificity $= TN/(TN+FP)$: quantifying the ability of the models to detect True Negative values;
- Precision $= TP/(TP+FP)$: quantifying the ability of the models to not produce False Positive values. At 1 no False positive was detected;
- Negative Value Precision (NPV) $= TN/(TN+FN)$: quantifying the ability of the models to not produce False Negative values. At 1 no False Negative was detected.
- Accuracy $= (TP+TN)/(TP+TN+FP+FN)$: proportion of correct detections over all measurements.
- Balanced Accuracy (BA) $(Sensitivity+Specificity)/2$: quantifying precision of the models. By construction, the BA is exactly 0.5 for the random no-skill model. In short, BA > 0.5 for a model means that this model has more skill than the random no-skill model.

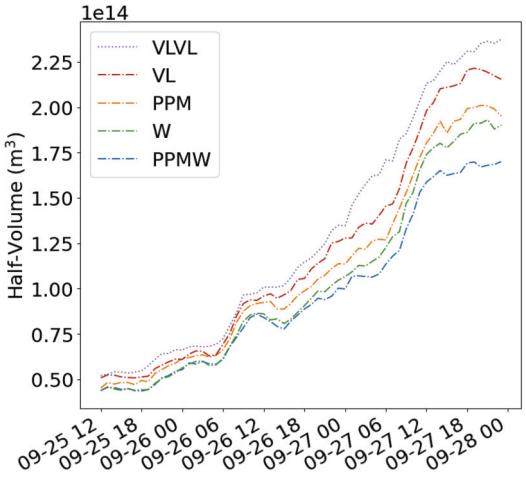

Fig. 2. Half-Volume of the ^{106}Ru plume as a function of time in the CHIMERE simulations defined in Table 2 for the firsts few days of simulations. Dotted line represents a simulation using Van Leer vertical advection scheme. Dash-dotted lines represent simulations using Deprés-Lagoutière vertical advections scheme.

All those indicators vary between 0 and 1, 1 representing best performance possible for the indicators.

We also computed Matthews correlation coefficient (MCC) (Matthews, 1975; Baldi et al., 2000) and the bias (Stephenson, 2000). The MCC varies between -1 (complete disagreement) and 1 (total agreement) and a random model will score 0. With the confusion matrices it is defined in equation (1). The MCC is a particularly reliable indicator in the case of a two-class confusion matrix (Chicco et al., 2021).

$$\Phi = \frac{(TP \times TN) - (FP \times FN)}{\sqrt{(TP+FP)(TP+FN)(TN+FP)(TN+FN)}} \quad (1)$$

The bias is defined as $B = \frac{TP+FP}{TP+FN}$ (Stephenson (2000)). The bias is zero by construction in the random no-skill model, but not in the simulations.

3. Results

In this section we will determine if numerical diffusion is effectively decreased by using specific numerical resolution schemes for transport (3.1). We will then compare the behavior of CHIMERE and FLEXPART on our test case. On one hand to identify any discrepancies due to the numerical diffusion (3.2). On the second hand to compare models performances to reflect the reality of the available data (3.3).

3.1. Alleviating Eulerian diffusion in CHIMERE

Before comparing the CHIMERE simulations with observations and with the FLEXPART simulations, comparing these simulations with each other is needed to quantify the differences in numerical diffusion depending on the advection schemes used (see Table 2). For this purpose, we will use time-series of the half-volume which, as discussed earlier, is a measure of numerical diffusion.

Fig. 2 shows the calculated half-volumes for all the simulations listed in Table 2. Comparing simulation VLVL with simulation VL, we observe that the use of the Deprés-Lagoutière scheme for vertical advection scheme systematically reduces the half-volume compared to the Van Leer scheme, as already observed in Lachatre et al. (2020) in the context of a volcanic plume from the Etna volcano. Regarding the impact of horizontal advection schemes, the results shown in Fig. 2 show that the PPM+W scheme is the less diffusive of all the tested horizontal scheme. The Walcek scheme is less diffusive than the PPM scheme in this case, while the Van Leer scheme yields the strongest half-volume all along the simulation. These results are consistent with the results

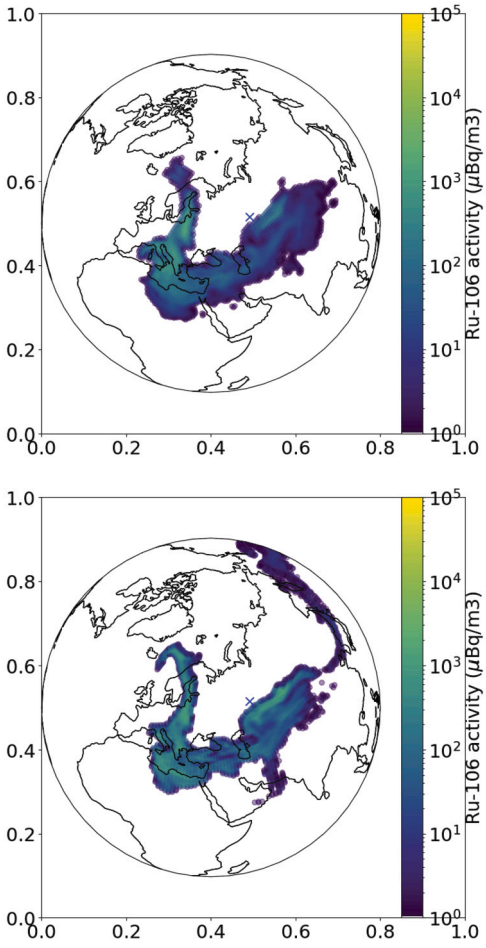

Fig. 3. ^{106}Ru plume on the 10th of October 2017 at 7 pm, a few days after the emission, as simulated with CHIMERE (top, PPMW) and FLEXPART (bottom). Colors represent the simulated activity concentrations integrated over vertical column of ^{106}Ru in μBq.m^{-3}. Only concentrations over 1 μBq.m^{-3} are represented. Blue cross is the origin of the emission in our scenario.

obtained by Mailler et al. (2023b) in an academic framework (their Fig. 8c). The configuration with minimal numerical diffusion among the 5 CHIMERE simulations is the PPM+W simulation, with the Després-Lagoutière scheme for vertical advection and the newly implemented PPM+W scheme for horizontal advection. In the next section, this simulation will be compared in detail to a FLEXPART simulation.

3.2. Comparison of diffusion between CHIMERE and FLEXPART

This paragraph aims to compare the half volume computed for CHIMERE and FLEXPART simulations. This will estimate the over diffusion emerging from the numerical resolution of the advection in CHIMERE.

Fig. 3 shows the simulated plume with our models on the 10th of October 2017 in the PPMW simulation with CHIMERE and in the FLEXPART simulation. At that date, the CHIMERE and FLEXPART simulations are consistent with each other. They depict a ^{106}Ru plume present over large parts of Europe, Asia and the Mediterranean basin, from Sweden and Norway in the North to Lybia and Egypt in the South, and from Italy to the West to central Asia to the East. At this date, some differences are also visible between the CHIMERE simulation and the FLEXPART simulation: in some areas of the plume (Scandinavia, North Africa, the Western Mediterranean Basin and the Middle-East), it seems to be spread over larger surfaces in CHIMERE than in FLEXPART, suggesting more diffusion in CHIMERE than in FLEXPART. It is also visible in certain areas that the simulated plume is more concentrated

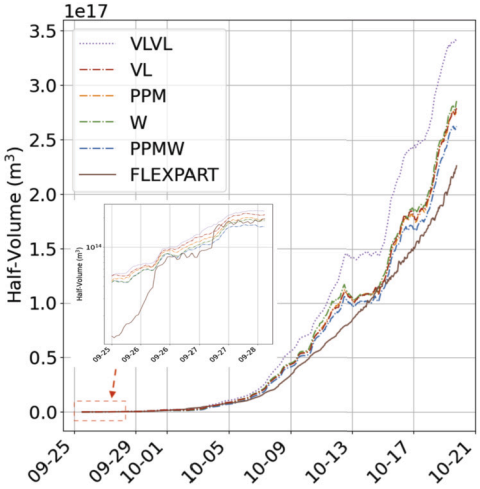

Fig. 4. Half-volume calculated for the models we used. Dotted line represents a simulation using Van Leer vertical advection scheme. Dash-dotted lines represent simulations using Deprés-Lagoutière vertical advections scheme. Continuous line represents the FLEXPART simulation. Insert highlights the first few days with a logarithmic scale for Y-axis.

in FLEXPART than in CHIMERE, reaching stronger activity concentrations values, for example over Scandinavia and the Arctic ocean. On the other hand, in the FLEXPART simulation, the plume reaches places from which it is absent in the CHIMERE simulation, for example over the Pacific and Indian oceans, while on the other hands the plume extends over the Western mediterranean sea in CHIMERE but not in FLEXPART. The map comparison at that date is therefore twofold regarding numerical diffusion, with visibly less spread of the plume in FLEXPART over certain areas, but visibly more spread in other areas.

To compare quantitatively diffusion between CHIMERE and FLEXPART, the half-volume time-series for FLEXPART and for the 5 CHIMERE simulations are presented in Fig. 4 over the total simulated period. First, we observe that the general evolution of the half-volume is very similar in all the CHIMERE simulations and in FLEXPART. In the second part of the simulations, from 2017-10-05, the FLEXPART simulation has a systematically smaller half-volume than the CHIMERE simulations. It is also visible that all along the simulations the vertical advection scheme in CHIMERE has a significant impact on the numerical diffusion in CHIMERE, with the VLVL simulation having a systematically higher half-volume than other CHIMERE simulations all along the numerical experiment, while in the second half of the simulations (starting around 2017-10-05) the time series corresponding to different horizontal schemes in CHIMERE (VL, W, PPM, PPMW) become very close to each other. Therefore, the half-volume time series in Fig. 4 shows that, for the first 10 days after the ^{106}Ru emission episode, additional diffusion in CHIMERE compared to FLEXPART is not systematic. Later on, the CHIMERE simulations systematically exhibit a half-volume slightly stronger than the FLEXPART simulation, and it is clearly visible than the use of the antidiffusive Després-Lagoutière scheme in the vertical direction reduces much of this gap, while the choice of less diffusive schemes for horizontal advection seems to be less important in the long run. We will check in 3.3 if that impact negatively the performances of the models.

3.3. Impact of the diffusion

In this section we will discuss what is the impact of the numerical diffusion of CHIMERE over the model performances in a practical situation.

In order to verify performances of our simulations, we propose to compare CHIMERE and FLEXPART simulations over our test case and the measurements. For each location in (Masson et al., 2019) we ana-

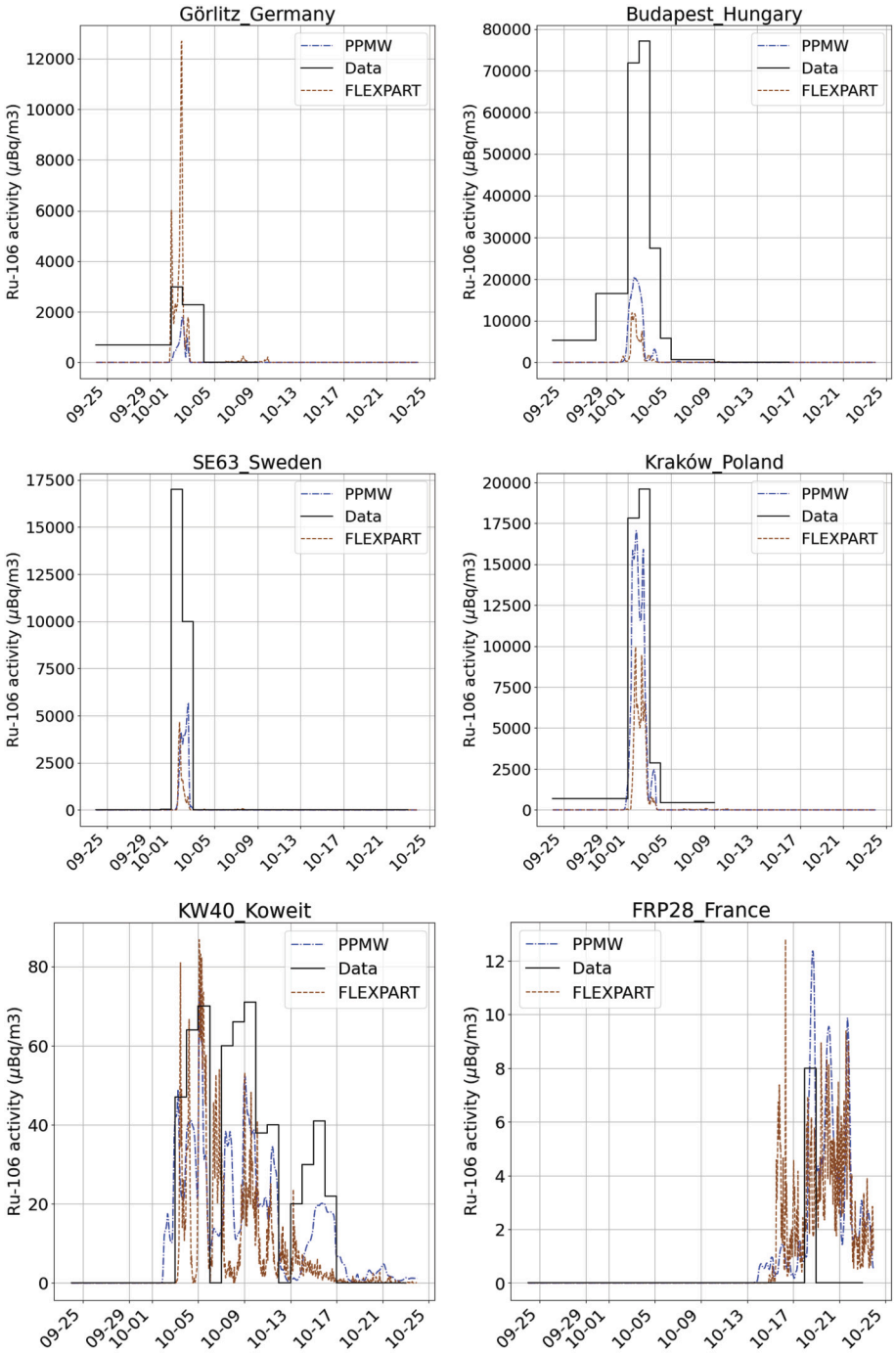

Fig. 5. Time series of activity concentration of ^{106}Ru in a measurement station located in Stockholm (Sweden). Black is the measurements, blue is simulated activity concentration in CHIMERE simulation labelled PPMW, brown in Flexpart.

lyzed time series of the detection of ^{106}Ru for all our simulations and for measurements. A few examples of the 337 time series we checked are presented in Fig. 5.

The main observations we extracted from them are: temporally all the simulations are in agreement between each others and most importantly in agreement with measurements. In term of activity concentrations there is more discrepancy (Görlitz time series for example) but that was to be expected because of the fundamental differences between the models and the unknown around the granularity of the aerosol. Though the activity concentration in all simulations stays in the same order of magnitude. Compared to measurements, it varies also quite a bit. In Budapest, simulation underestimate largely the concentrations but in Krakow they are in good agreement.

Moreover for the well defined peaks of measured activity concentrations, for example in Sweden and Poland (middle row of Fig. 5), we observed also well defined main peaks in our simulations. The hourly precision in our simulations allows to show finer variations (three peaks for the Polish station) that we can't always confirm with the measurements done with longer sampling time, but appears in both models. On the other hand the Hungarian and Polish stations measurements are in agreement for respectively the second and third smaller peaks observed in our simulations

We were especially interested in the behavior of our models for longer travel distances. The FRP28 IMS station located in Guadeloupe is thus a valuable comparison test for our model. Our simulations show a nosier output for FLEXPART and a blunted one for CHIMERE. Both

Table 6
Confusion matrices for FLEXPART, PPMW, PPM, W, VL and VLVL simulations.

		Measured			Measured			Measured	
	FLEX	Yes	No	*PPMW*	Yes	No	*PPM*	Yes	No
Model	Yes	345	286	Yes	341	108	Yes	342	116
	No	169	540	No	173	718	No	172	710
	W	Yes	No	*VL*	Yes	No	*VLVL*	Yes	No
Model	Yes	349	150	Yes	335	104	Yes	335	102
	No	165	676	No	179	722	No	179	724

were expected because of the low level of activity left due to deposition occurring since a month already. The IMS Koweit station (KW40) in Fig. 5 shows those observations. Again both model are behaving similarly and the highest simulated activity concentration for the CHIMERE simulation happened at the correct time.

IMS stations' measurements are done daily making them a valuable asset for a comparison of time-series. When analyzing the time-series, the KW40 IMS stations presented three detections episodes separated by a 24 h time window with no detections. Our simulations reproduced these three main periods separated by a lower simulated activity concentration in between. As mention before the longer time passed the noisier the simulations get. In the case of KW40 we can see that the quality of the successive episodes decreased, with a higher degradation in the case of the FLEXPART simulation. In the CHIMERE simulation the last episode is very round peak compared to the first two with multiple sharper peaks. This blunted third peak might be an observable effect of the Eulerian diffusion.

Time-series on locations of the measurements stations give a general outlook on performances. It indicates that models are in good agreement with each other and with the measurements. Next section will present results for an objective comparison based on skill scores.

3.4. Objective indicators comparison

To get an objective comparison of performances we calculate the confusion matrices for all the simulations as described in section 2. All confusion matrices are presented in Table 6. First point to note is that the confusion matrix of the FLEXPART simulation presents more FP than in all our CHIMERE simulations. Meaning that the total number of simulated positives value $P = TP + FP$ is higher than for any CHIMERE simulations. At this point that could further indicate, knowing that the half-volume of our CHIMERE simulation is bigger than FLEXPART's, that the tracer diffused more in CHIMERE and presents activity concentrations slightly lower than in FLEXPART's simulation and such going under our threshold value more often. That might indicate an impact on performances of CHIMERE.

Table 7 presents all calculated indicators for our models and the random model we presented in section 2.3. A few important points can be highlighted. First and foremost, all models perform better than the random no-skill for every indicator at the exception of the bias. Also, all the advection combinations tested with CHIMERE score better than FLEXPART with respect to the indicators. This indicates that in this particular case CHIMERE presents better performance in nearly all indicators (better hit rate, less false alarms), sensitivity of FLEXPART being the closest to CHIMERE simulations. Between the different advections schemes in CHIMERE no particular differences seem visible in term of scores except for the simulation utilizing the Walcek horizontal advections scheme, which seems slightly inferior to other CHIMERE simulations.

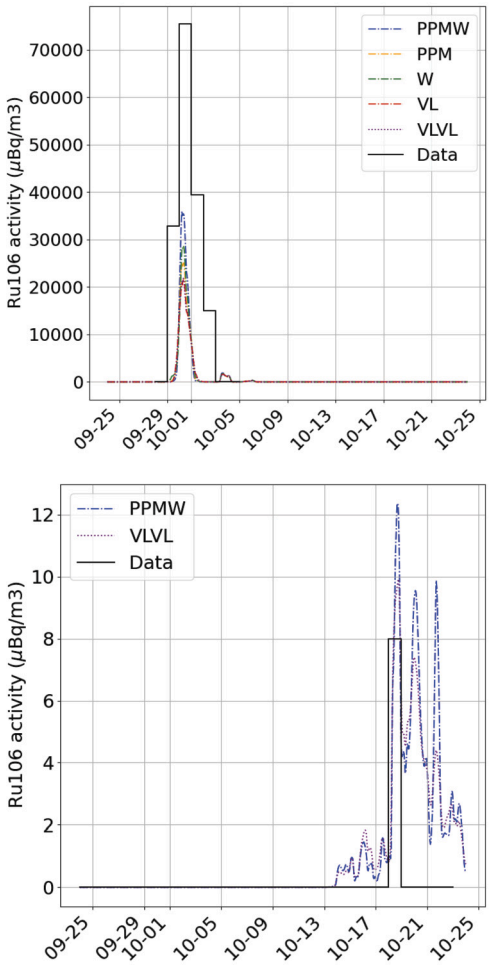

Fig. 6. Top: Comparison of time series of all advections schemes tested with CHIMERE on the station "Alba-Lulia, Romania" location. Bottom: Time series of FRP28 IMS station in Guadeloupe comparison between the least (PPMW) an most (VLVL) diffusive advections schemes tested with CHIMERE.

Fig. 6 shows time series of the simulated activity concentrations over station Alt-Perau (Austria) for all the CHIMERE simulations. In this time series, we see that the choice of advection schemes changes strongly the intensity of the simulated peaks, where peak obtained with the less diffusive model configuration (PPM+W) is about 50% stronger than in the most diffusive model configurations. Comparing these time series with Fig. 2 makes sense, since we observe that the schemes representing the smallest half-volumes for the plumes (PPM+W, Walcek, PPM)

Table 7
Performances indicators for all simulations. Bold is for best performances in the tested models and italic is for the worst, random no-skill model excluded.

Label	Bias	Sensitivity	Specificity	Precision	NPV	Accuracy	Baccuracy	MCC
VLVL	*0.850*	*0.652*	**0.877**	**0.767**	0.802	**0.790**	0.764	0.548
VL	0.854	*0.652*	0.874	0.763	0.801	0.789	0.763	0.545
PPM	0.891	0.665	0.860	0.747	0.805	0.785	0.762	0.538
W	**0.971**	**0.679**	0.818	0.699	0.804	0.765	0.749	0.500
PPMW	0.874	0.663	0.869	0.759	**0.806**	**0.790**	**0.766**	**0.549**
FLEXPART	1.228	0.671	*0.654*	*0.547*	*0.762*	*0.660*	*0.662*	*0.317*
RANDOM	1.000	0.384	0.616	0.384	0.616	0.527	0.500	0.000

Table 8
Performances indicators for all simulations for our three threshold values. Bold is for best performances in the tested models and italic is for the worst, for each threshold.

	Threshold	Bias	Sensitivity	Specificity	Precision	NPV	Accuracy	Baccuracy	MCC
	5	0.860	*0.652*	**0.870**	**0.758**	0.801	**0.787**	**0.761**	**0.540**
VLVL	10	0.850	*0.652*	**0.877**	**0.767**	0.802	**0.790**	0.764	0.548
	15	0.844	*0.648*	**0.878**	0.767	0.800	**0.790**	0.763	**0.546**
	5	0.866	0.652	0.867	0.753	0.800	0.784	0.759	0.535
VL	10	0.854	*0.652*	0.874	0.763	0.801	0.789	0.763	0.545
	15	0.846	0.650	0.878	**0.768**	0.801	**0.790**	0.764	**0.548**
	5	0.918	0.671	0.846	0.731	**0.805**	0.779	0.759	0.527
PPM	10	0.891	0.665	0.860	0.747	0.805	0.785	0.762	0.538
	15	0.866	0.660	0.872	0.762	**0.804**	**0.790**	**0.766**	**0.548**
	5	**0.992**	**0.679**	0.805	0.684	0.801	0.757	0.742	0.485
W	10	**0.971**	**0.679**	0.818	0.699	0.804	0.765	0.749	0.500
	15	**0.938**	**0.677**	0.838	0.722	**0.807**	0.776	0.757	0.522
	5	0.914	0.669	0.847	0.732	0.805	0.779	0.758	0.527
PPMW	10	0.874	0.663	0.869	0.759	**0.806**	**0.790**	**0.766**	**0.549**
	15	0.864	0.658	0.872	0.761	0.804	**0.790**	0.765	0.547
	5	*1.263*	0.683	*0.639*	*0.541*	*0.764*	*0.656*	*0.661*	*0.313*
FLEX	10	*1.228*	0.671	*0.654*	*0.547*	*0.762*	*0.660*	*0.662*	*0.317*
	15	*1.208*	0.658	*0.657*	*0.544*	*0.755*	*0.657*	*0.657*	*0.307*

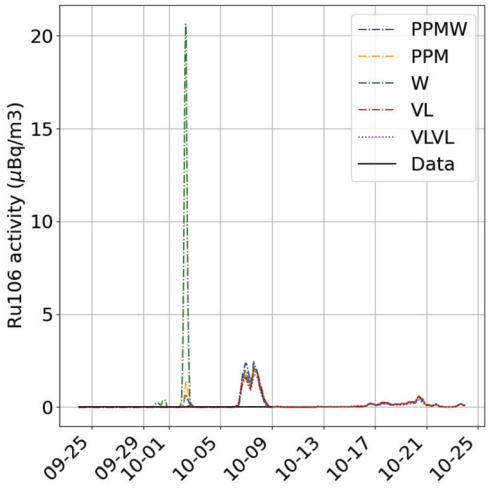

Fig. 7. Example of time series where the Walcek advection scheme presents a false positive peak and the other CHIMERE advections schemes do not. Measurement station is in Würzburg, Germany.

are also the ones representing the strongest peaks. Fig. 6b shows the time series for the less diffusive simulation (PPM+W) and for the most diffusive, for IMS station FRP28, in the French overseas territory of Guadeloupe. Many characteristics of the simulations can be observed on this time series: first, both simulations have their first significant peak at the time of detection of the plume by the IMS station. However, both models go past the threshold value of 10 μBq m^{-3} once or twice in the days following the detection, which is considered as a "false alarm" (FP) in the confusion matrices. Regarding the peak intensity, we observe as Fig. 6a that the peaks are stronger in the less diffusive simulation (PPM+W), and weaker in the most diffusive one (VLVL), while the minima in-between two peaks are lower in the PPM+W simulation: the less diffusive simulation, characterized by a smaller half-volume (Fig. 2) has sharper peaks, more clearly separated from each other. Another point worth mentioning is the lower performances observed for the Walcek horizontal advection scheme compared to the other schemes in CHIMERE. We checked on every time series at our disposal and remarked that, over certain stations, this specific simulation presents false detection peaks where the other ones do not. Fig. 7 shows an example of said false positive peaks. That confirms the value differences in Table 7, especially in term of bias and sensitivity, and suggests that, while less diffusive than Van Leer and even than PPM, the Walcek scheme may underperform these schemes in certain situations, in a way sufficiently significant to substantially degrade its scores against other advection schemes (Table 7).

To comfort our first observation that CHIMERE performs better than FLEXPART in this particular case, we decided to test the robustness of our choice for our thresholding method. We tested a lower (5 μBq m^{-3}) and a higher (15 μBq m^{-3}) threshold values for our analysis. Results are shown in Table 8. All indicators do not vary significantly with the different thresholds tested. The best and worst model performances do not vary much either. We also tested the impact of the meteorology by using the same WRF files we used for our CHIMERE simulations as input in a version of FLEXPART capable of using them as input (Brioude et al., 2013). We used the exact same parameters as in the FLEXPART simulation we presented. We observed small improvements in the scores between the two FLEXPART simulations when using the WRF calculated meteorology but our conclusions remain. All scores we calculated clearly show that an Eulerian model like CHIMERE can be adapted to simulate advection of radioisotope plumes over long distances and long times, and can perform better than a Lagrangian model compared to observations on a uncontrolled pollution case.

4. Conclusions

The main goal of this study was to evaluate the capability of two models, Eulerian and Lagrangian, including several transport schemes to accurately model a specific radionuclides transport event. The studied case corresponds to the release of an unique tracer, ^{106}Ru, on 24th of September 2017. It means that the corresponding measurements, when non-zero values are measured, are necessarily relative to this unique release. First, the simulations showed that the hypothesis about the location and the timing was correct and realistic. By construction, the Eulerian model is more diffusive than the Lagrangian one, and this was quantified on this test case. A sensitive point was to show that the use of the Després and Lagoutière (1999) scheme enables to reduce the differences between the two models. The benefit of this scheme on the vertical remain during the whole simulation, when the benefit of various more or less horizontal advection schemes, is mainly obtained just after the release, when concentrations are important. Finally, tests with several schemes showed that the combination of DPL, vertically, and PPM+W, horizontally enables to have results of same shape that with

the use of Lagrangian model. It means that with this transport scheme, it is possible to keep the advantages of a Lagrangian model (reduced numerical diffusion) but also benefit of all capabilities of an Eulerian scheme.

The present study also shows that in a comparison with realistic data and measurement conditions (sparse measurements in time and location, and a wide range of sampling time reacting to an unexpected event) both approaches were yielding better results and performances than a random model. Overall CHIMERE proposed better performances on this applied case than FLEXPART for all eight indicators we computed and for all the tested combinations of numerical advection schemes. At the exception of the Walcek horizontal advection scheme, all CHIMERE advection schemes scored quite comparatively with each other. Between the best overall (best in 6 out of 8 indicators) scoring advection schemes combination (VLVL) and the least diffusive (PPMW) differences of scores are extremely close, only 0.002 of differences for BAccurracy for example. The Walcek horizontal advection scheme despite being less diffusive in our analysis than the best scoring advection schemes (VLVL), presents a small supplementary amount of False Positive peaks than the other numerical schemes for transport on our test case.

Even knowing that scores depend on multiple parameters we hoped that reducing numerical diffusion would suffice to improve the scoring. Turns out that was not the case in our study. Neither was there a large degradation of scores between the advection schemes tested. It leads us to conclude that reducing the numerical diffusion does not directly imply better scores and that changing advections schemes have a more complex impact on scores than anticipated. Other parameters might have a bigger impact on performances for both model for example the aerosol representation. Future works might greatly benefit of a more precise and better constrained granularity of the aerosol considered, especially in the context of an accidental release. The deposition has an impact on performances for this case in our models (obviously as it is the only sink for the aerosol). We fixed the distribution of size of the aerosol in our simulation to being a monodispersive Gaussian distribution centered and calibrated to allow our simulations to demonstrate, on farther stations (FRP28 in Guadeloupe and USP72 in Florida), a data coherent result. A better knowledge on the aerosol size distribution might lead to better performances in the models and thus on future risk assessment analysis. Furthermore this paper only takes into account the atmospheric transport part of our model but as an Eulerian model CHIMERE could bring even more information on more complex cases involving complex chemistry or radioactive decay chains.

Another consideration not developed in this study is the response time to an accidental release. This kind of models can be used for emergency procedures, mostly when there is a suspicion of a nuclear accident and one wants to be able to simulate the most likely transport very quickly. On this particular event and with our computing power, with FLEXPART we can simulate a 24 hours period with 1 processor in about 1 hour. For the same simulated period we need around 45 minutes but using 60 processors with CHIMERE, assuming meteorology calculations are done or not needed (using ECMWF files as input for example). If CHIMERE is capable of bringing a more complex answer on a given problem, FLEXPART on the other hand is a very efficient tool to give an answer faster, especially if computational power is limited. Conjoint use might lead to interesting results in future cases and studies: using FLEXPART as a “First-responder” or to rapidly explore parameters spaces (for example aerosol physical description) and CHIMERE as an more in depth “Investigator” or for re-analysis of past events as presented in this study.

Ethical statement

This article does not contain any studies with human participant nor animal performed by any of the authors.

CRediT authorship contribution statement

Léo Adenis: Writing – review & editing, Writing – original draft, Visualization, Validation, Software, Methodology, Investigation, Formal analysis, Data curation, Conceptualization. **Sylvain Mailler:** Writing – review & editing, Writing – original draft, Supervision, Software, Project administration, Funding acquisition, Formal analysis, Conceptualization. **Laurent Menut:** Writing – review & editing, Validation, Supervision, Software, Resources, Methodology, Data curation, Conceptualization. **Pascal Achim:** Writing – review & editing, Supervision, Project administration, Funding acquisition, Conceptualization. **Sylvia Generoso:** Writing – review & editing, Supervision, Software, Resources, Data curation.

Declaration of competing interest

The authors declare that they have no known competing financial interests or personal relationships that could have appeared to influence the work reported in this paper.

Data availability

The CHIMERE v2020 model is available on its dedicated web site https://www.lmd.polytechnique.fr and for download at https://doi.org/10.14768/8afd9058-909c-4827-94b8-69f05f7bb46d. The open-source codes for the FLEXPART (v9.0.2) model is accessible at https://www.flexpart.eu/downloads.

Acknowledgements

We thank the OASIS modeling team for their support with the OASIS coupler, the WRF developers team for the free use of their model and the investigators and staff who maintain and provide the AERONET data (https://aeronet.gsfc.nasa.gov/). European Environmental Agency (EEA) is acknowledged for their air quality station data that is provided and freely downloadable (https://www.eea.europa.eu/data-and-maps/data/aqereporting-8). This work was funded by LRC Yves-Rocard (Laboratoire de Recherche Conventionné CEA-ENS-CNRS).

References

Baldi, P., Brunak, S., Chauvin, Y., Andersen, C.A.F., Nielsen, H., 2000. Assessing the accuracy of prediction algorithms for classification: an overview. Bioinformatics 16 (5), 412–424. https://doi.org/10.1093/bioinformatics/16.5.412.

Briant, R., Tuccella, P., Deroubaix, A., Khvorostyanov, D., Menut, L., Mailler, S., Turquety, S., 2017. Aerosol–radiation interaction modelling using online coupling between the WRF 3.7.1 meteorological model and the CHIMERE 2016 chemistry-transport model, through the OASIS3-MCT coupler. Geosci. Model Dev. 10 (2), 927–944. https://doi.org/10.5194/gmd-10-927-2017. https://gmd.copernicus.org/articles/10/927/2017/.

Brioude, J., Arnold, D., Stohl, A., Cassiani, M., Morton, D., Seibert, P., Angevine, W., Evan, S., Dingwell, A., Fast, J.D., Easter, R.C., Pisso, I., Burkhart, J., Wotawa, G., 2013. The Lagrangian particle dispersion model FLEXPART-WRF version 3.1. Geosci. Model Dev. 6 (6), 1889–1904. https://doi.org/10.5194/gmd-6-1889-2013. https://gmd.copernicus.org/articles/6/1889/2013/.

Brunner, D., 2012. Atmospheric Chemistry in Lagrangian Models—Overview. Chap. 19. American Geophysical Union (AGU), pp. 224–234. https://agupubs.onlinelibrary.wiley.com/doi/abs/10.1029/2012GM001431.

Byun, D., Schere, K.L., 2006. Review of the governing equations, computational algorithms, and other components of the models-3 community multiscale air quality (CMAQ) modeling system. Appl. Mech. Rev. 59 (2), 51–77. https://doi.org/10.1115/1.2128636.

Chicco, D., Tötsch, N., Jurman, G., 2021. The Matthews correlation coefficient (MCC) is more reliable than balanced accuracy, bookmaker informedness, and markedness in two-class confusion matrix evaluation. BioData Min. 14 (1), 13. https://doi.org/10.1186/s13040-021-00244-z. https://biodatamining.biomedcentral.com/articles/10.1186/s13040-021-00244-z.

Colella, P., Woodward, P.R., 1984. The piecewise parabolic method (PPM) for gas-dynamical simulations. J. Comput. Phys. 54 (1), 174–201. https://doi.org/10.1016/0021-9991(84)90143-8. https://linkinghub.elsevier.com/retrieve/pii/0021999184901438.

Després, B., Lagoutière, F., 1999. Un schéma non linéaire anti-dissipatif pour l'équation d'advection linéaire. C. R. Acad. Sci., Ser. 1 Math. 328 (10), 939–943. https://doi.org/10.1016/S0764-4442(99)80301-2. https://www.sciencedirect.com/science/article/pii/S0764444299803012.

Dumont Le Brazidec, J., Bocquet, M., Saunier, O., Roustan, Y., 2020. MCMC methods applied to the reconstruction of the autumn 2017 Ruthenium-106 atmospheric contamination source. Atmos. Environ. X 6, 100,071. https://doi.org/10.1016/j.aeaoa.2020.100071. https://linkinghub.elsevier.com/retrieve/pii/S2590162120300101.

Dumont Le Brazidec, J., Bocquet, M., Saunier, O., Roustan, Y., 2021. Quantification of uncertainties in the assessment of an atmospheric release source applied to the autumn 2017 ^{106}ru event. Atmos. Chem. Phys. 21 (17), 13,247–13,267. https://doi.org/10.5194/acp-21-13247-2021. https://acp.copernicus.org/articles/21/13247/2021/.

Eastham, S.D., Jacob, D.J., 2016. Limits on the ability of global Eulerian models to resolveintercontinental transport of chemical plumes. Preprint. Dynamics/Atmospheric Modelling/Troposphere/Physics (physical properties and processes). https://doi.org/10.5194/acp-2016-943. https://acp.copernicus.org/preprints/acp-2016-943/acp-2016-943.pdf, 2016.

Fawcett, T., 2006. An introduction to ROC analysis. Pattern Recognit. Lett. 27 (8), 861–874. https://doi.org/10.1016/j.patrec.2005.10.010. https://linkinghub.elsevier.com/retrieve/pii/S016786550500303X.

Freitas, S.R., Rodrigues, L.F., Longo, K.M., Panetta, J., 2012. Impact of a monotonic advection scheme with low numerical diffusion on transport modeling of emissions from biomass burning. J. Adv. Model. Earth Syst. 4 (1). https://doi.org/10.1029/2011MS000084. https://agupubs.onlinelibrary.wiley.com/doi/abs/10.1029/2011MS000084.

Godunov, S.K., 1959. Finite difference method for numerical computation of discontinuous solutions of the equations of fluid dynamics. Mat. Sb. 47(89) (3), 271–306. https://hal.archives-ouvertes.fr/hal-01620642.

Henne, S., Poberaj, C.S., Reimann, S., Brunner, D., 2013. Global-scale tropospheric Lagrangian particle models with linear chemistry. In: Lin, J., Brunner, D., Gerbig, C., Stohl, A., Luhar, A., Webley, P. (Eds.), Lagrangian Modeling of the Atmosphere. In: Geophysical Monograph Series. American Geophysical Union, Washington, D.C., pp. 235–250. http://doi.wiley.com/10.1029/2012GM001247.

Hersbach, H., 2019. Global reanalysis: goodbye era-interim, hello ERA5. https://cir.nii.ac.jp/crid/1370009142513757452.

Hertel, O., Christensen, J., Runge, E.H., Asman, W.A., Berkowicz, R., Hovmand, M.F., Hov, Ø., 1995. Development and testing of a new variable scale air pollution model—ACDEP. Atmos. Environ. 29 (11), 1267–1290. https://doi.org/10.1016/1352-2310(95)00067-9. https://linkinghub.elsevier.com/retrieve/pii/1352231095000679.

Jones, A., Thomson, D., Hort, M., Devenish, B., 2007. The U.K. Met office's next-generation atmospheric dispersion model, NAME III. In: Borrego, C., Norman, A.L. (Eds.), Air Pollution Modeling and Its Application XVII. Springer US, Boston, MA, pp. 580–589.

Lachatre, M., Mailler, S., Menut, L., Cholakian, A., Sellitto, P., Siour, G., Guermazi, H., Salerno, G., Giammanco, S., 2022. Modelling SO_2 conversion into sulfates in the mid-troposphere with a 3D chemistry transport model: the case of Mount Etna's eruption on 12 April 2012. Atmos. Chem. Phys. 22 (20), 13,861–13,879. https://doi.org/10.5194/acp-22-13861-2022. https://acp.copernicus.org/articles/22/13861/2022/.

Lachatre, M., Mailler, S., Menut, L., Turquety, S., Sellitto, P., Guermazi, H., Salerno, G., Caltabiano, T., Carboni, E., 2020. New strategies for vertical transport in chemistry transport models: application to the case of the Mount Etna eruption on 18 March 2012 with CHIMERE v2017r4. Geosci. Model Dev. 13 (11), 5707–5723. https://doi.org/10.5194/gmd-13-5707-2020. https://gmd.copernicus.org/articles/13/5707/2020/.

van Leer, B., 2003. Upwind and high-resolution methods for compressible flow: from donor cell to residual-distribution schemes. https://doi.org/10.2514/6.2003-3559.

Mailler, S., Menut, L., Cholakian, A., Pennel, R., 2023a. Aersett v1.0: a simple and straightforward model for the settling speed of big spherical atmospheric aerosols. Geosci. Model Dev. 16 (3), 1119–1127. https://doi.org/10.5194/gmd-16-1119-2023. https://gmd.copernicus.org/articles/16/1119/2023/.

Mailler, S., Pennel, R., 2023. toyCTM. https://doi.org/10.5281/zenodo.7824831.

Mailler, S., Pennel, R., Menut, L., Cholakian, A., 2023b. An improved version of the piecewise parabolic method advection scheme: description and performance assessment in a bidimensional testcase with stiff chemistry in toyCTM v1.0. Geosci. Model Dev. Discuss.

Mailler, S., Pennel, R., Menut, L., Lachâtre, M., 2021. Using the Després and Lagoutière (1999) antidiffusive transport scheme: a promising and novel method against excessive vertical diffusion in chemistry-transport models. Geosci. Model Dev. 14 (4), 2221–2233. https://doi.org/10.5194/gmd-14-2221-2021. https://gmd.copernicus.org/articles/14/2221/2021/.

Mallios, S.A., Daskalopoulou, V., Amiridis, V., 2021. Orientation of non spherical prolate dust particles moving vertically in the earth's atmosphere. J. Aerosol Sci. 151, 105,657. https://doi.org/10.1016/j.jaerosci.2020.105657. https://www.sciencedirect.com/science/article/pii/S0021850220301427.

Mallios, S.A., Drakaki, E., Amiridis, V., 2020. Effects of dust particle sphericity and orientation on their gravitational settling in the earth's atmosphere. J. Aerosol Sci. 150, 105,634. https://doi.org/10.1016/j.jaerosci.2020.105634. https://www.sciencedirect.com/science/article/pii/S0021850220301208.

Martin, R.V., Eastham, S.D., Bindle, L., Lundgren, E.W., Clune, T.L., Keller, C.A., Downs, W., Zhang, D., Lucchesi, R.A., Sulprizio, M.P., Yantosca, R.M., Li, Y., Estrada, L., Putman, W.M., Auer, B.M., Trayanov, A.L., Pawson, S., Jacob, D.J., 2022. Improved advection, resolution, performance, and community access in the new generation (version 13) of the high-performance GEOS-Chem global atmospheric chemistry model (GCHP). Geosci. Model Dev. 15 (23), 8731–8748. https://doi.org/10.5194/gmd-15-8731-2022.

Masson, O., Steinhauser, G., Zok, D., Saunier, O., Angelov, H., Babić, D., Bečková, V., Bieringer, J., Bruggeman, M., Burbidge, C.I., Conil, S., Dalheimer, A., De Geer, L.E., de Vismes Ott, A., Eleftheriadis, K., Estier, S., Fischer, H., Garavaglia, M.G., Gasco Leonarte, C., Gorzkiewicz, K., Hainz, D., Hoffman, I., Hýža, M., Isajenko, K., Karhunen, T., Kastlander, J., Katzlberger, C., Kierepko, R., Knetsch, G.J., Kövendiné Kónyi, J., Lecomte, M., Mietelski, J.W., Min, P., Møller, B., Nielsen, S.P., Nikolic, J., Nikolovska, L., Penev, I., Petrinec, B., Povinec, P.P., Querfeld, R., Raimondi, O., Ransby, D., Ringer, W., Romanenko, O., Rusconi, R., Saey, P.R.J., Samsonov, V., Šilobritienė, B., Simion, E., Söderström, C., Šoštarić, M., Steinkopff, T., Steinmann, P., Sýkora, I., Tabachnyi, L., Todorovic, D., Tomankiewicz, E., Tschiersch, J., Tsibranski, R., Tzortzis, M., Ungar, K., Vidic, A., Weller, A., Wershofen, H., Zagyvai, P., Zalewska, T., Zapata García, D., Zorko, B., 2019. Airborne concentrations and chemical considerations of radioactive ruthenium from an undeclared major nuclear release in 2017. Proc. Natl. Acad. Sci. USA 116 (34), 16,750–16,759. https://doi.org/10.1073/pnas.1907571116. https://pnas.org/doi/full/10.1073/pnas.1907571116.

Matthews, B., 1975. Comparison of the predicted and observed secondary structure of T4 phage lysozyme. Biochim. Biophys. Acta, Protein Struct. 405 (2), 442–451. https://doi.org/10.1016/0005-2795(75)90109-9. https://linkinghub.elsevier.com/retrieve/pii/0005279575901099.

McMahon, T., Denison, P., 1979. Empirical atmospheric deposition parameters—a survey. Atmos. Environ. 13 (5), 571–585. https://doi.org/10.1016/0004-6981(79)90186-0. https://linkinghub.elsevier.com/retrieve/pii/0004698179901860.

Menut, L., Bessagnet, B., Briant, R., Cholakian, A., Couvidat, F., Mailler, S., Pennel, R., Siour, G., Tuccella, P., Turquety, S., Valari, M., 2021. The CHIMERE v2020r1 online chemistry-transport model. Geosci. Model Dev. 14 (11), 6781–6811. https://doi.org/10.5194/gmd-14-6781-2021. https://gmd.copernicus.org/articles/14/6781/2021/.

National Centers for Environmental Prediction, National Weather Service, NOAA, U.S. Department of Commerce. NCEP FNL operational model global tropospheric analyses, continuing from July 1999. https://doi.org/10.5065/D6M043C6.

Paatero, J., Kulmala, S., Jaakkola, T., Saxén, R., Buyukay, M., 2007. Deposition of ^{125}Sb, ^{106}Ru, ^{144}Ce, ^{134}Cs and ^{137}Cs in Finland after the Chernobyl accident. Boreal Environ. Res. 12, 43–54. http://www.borenv.net/BER/archive/pdfs/ber12/ber12-043.pdf.

Pailleux, J., Geleyn, J.F., Legrand, E., 2000. La prévision numérique du temps avec les modèles arpège et aladin-bilan et perspectives. Météorologie 2000 (30), 32–60.

Plu, M., Bigeard, G., Sič, B., Emili, E., Bugliaro, L., El Amraoui, L., Guth, J., Josse, B., Mona, L., Piontek, D., 2021. Modelling the volcanic ash plume from Eyjafjallajökull eruption (May 2010) over Europe: evaluation of the benefit of source term improvements and of the assimilation of aerosol measurements. Nat. Hazards Earth Syst. Sci. 21 (12), 3731–3747. https://doi.org/10.5194/nhess-21-3731-2021. https://nhess.copernicus.org/articles/21/3731/2021/.

Saunier, O., Didier, D., Mathieu, A., Masson, O., Dumont Le Brazidec, J., 2019. Atmospheric modeling and source reconstruction of radioactive ruthenium from an undeclared major release in 2017. Proc. Natl. Acad. Sci. USA 116 (50), 24,991–25,000. https://doi.org/10.1073/pnas.1907823116. https://pnas.org/doi/full/10.1073/pnas.1907823116.

Skamarock, W.C., Klemp, J.B., Dudhia, J., Gill, D.O., Barker, D.M., Duda, M.G., Huang, X.Y., Wang, W., Powers, J.G., 2008. A description of the advanced research WRF version 3. https://doi.org/10.5065/D68S4MVH.

Stephenson, D.B., 2000. Use of the "odds ratio" for diagnosing forecast skill. Weather Forecast. 15 (2), 221–232. https://doi.org/10.1175/1520-0434(2000)015<0221:UOTORF>2.0.CO;2.

Stohl, A., Sodemann, H., Eckhardt, S., Frank, A., Seibert, P., Wotawa, G., 2010. The Lagrangian particle dispersion model FLEXPART version 8.2, p. 33.

von Storch, H., Langenberg, H., Feser, F., 2000. A spectral nudging technique for dynamical downscaling purposes. Mon. Weather Rev. 128 (10), 3664–3673. https://doi.org/10.1175/1520-0493(2000)128<3664:ASNTFD>2.0.CO;2. http://journals.ametsoc.org/doi/10.1175/1520-0493(2000)128<3664:ASNTFD>2.0.CO;2.

Sørensen, J.H., 2018. Method for source localization proposed and applied to the October 2017 case of atmospheric dispersion of Ru-106. J. Environ. Radioact. 189, 221–226. https://doi.org/10.1016/j.jenvrad.2018.03.010. https://linkinghub.elsevier.com/retrieve/pii/S0265931X18300146.

Timmermans, R., van Pinxteren, D., Kranenburg, R., Hendriks, C., Fomba, K., Herrmann, H., Schaap, M., 2022. Evaluation of modelled LOTOS-EUROS with observational based PM10 source attribution. Atmos. Environ. X 14, 100,173. https://doi.org/10.1016/j.aeaoa.2022.100173. https://www.sciencedirect.com/science/article/pii/S2590162122000272.

Tombette, M., Quentric, E., Quélo, D., Benoit, J.P., Mathieu, A., Korsakissok, I., Didier, D., 2014. C3x: a software platform for assessing the consequences of an accidental release of radioactivity into the atmosphere. In: Poster Presented at Fourth European IRPA Congress, pp. 23–27.

Van Leer, B., 1977. Towards the ultimate conservative difference scheme. IV. A new approach to numerical convection. J. Comput. Phys. 23 (3), 276–299. https://doi.org/10.1016/0021-9991(77)90095-X. http://www.sciencedirect.com/science/article/pii/002199917790095X.

Walcek, C.J., 2000. Minor flux adjustment near mixing ratio extremes for simplified yet highly accurate monotonic calculation of tracer advection. J. Geophys. Res. 105 (D7), 9335–9348. https://doi.org/10.1029/1999JD901142.

Walters, D.N., Williams, K.D., Boutle, I.A., Bushell, A.C., Edwards, J.M., Field, P.R., Lock, A.P., Morcrette, C.J., Stratton, R.A., Wilkinson, J.M., Willett, M.R., Bellouin, N., Bodas-Salcedo, A., Brooks, M.E., Copsey, D., Earnshaw, P.D., Hardiman, S.C., Harris, C.M., Levine, R.C., MacLachlan, C., Manners, J.C., Martin, G.M., Milton, S.F., Palmer, M.D., Roberts, M.J., Rodríguez, J.M., Tennant, W.J., Vidale, P.L., 2014. The Met Office unified model global atmosphere 4.0 and JULES global land 4.0 configurations. Geosci. Model Dev. 7 (1), 361–386. https://doi.org/10.5194/gmd-7-361-2014. https://gmd.copernicus.org/articles/7/361/2014/.

Wang, X., Zhang, L., Moran, M.D., 2014. Development of a new semi-empirical parameterization for below-cloud scavenging of size-resolved aerosol particles by both rain and snow. Geosci. Model Dev. 7 (3), 799–819. https://doi.org/10.5194/gmd-7-799-2014. https://gmd.copernicus.org/articles/7/799/2014/.

Western, L.M., Millington, S.C., Benfield-Dexter, A., Witham, C.S., 2020. Source estimation of an unexpected release of Ruthenium-106 in 2017 using an inverse modelling approach. J. Environ. Radioact. 220–221, 106,304. https://doi.org/10.1016/j.jenvrad.2020.106304. https://linkinghub.elsevier.com/retrieve/pii/S0265931X20301636.

Willis, P.T., Tattelman, P., 1989. Drop-size distributions associated with intense rainfall. J. Appl. Meteorol. Climatol. 28 (1), 3–15. https://doi.org/10.1175/1520-0450(1989)028<0003:DSDAWI>2.0.CO;2. https://journals.ametsoc.org/view/journals/apme/28/1/1520-0450_1989_028_0003_dsdawi_2_0_co_2.xml.

Zhang, L., Gong, S., Padro, J., Barrie, L., 2001. A size-segregated particle dry deposition scheme for an atmospheric aerosol module. Atmos. Environ. 35 (3), 549–560. https://doi.org/10.1016/S1352-2310(00)00326-5. https://www.sciencedirect.com/science/article/pii/S1352231000003265.

Zhao, S., Russell, M.G., Hakami, A., Capps, S.L., Turner, M.D., Henze, D.K., Percell, P.B., Resler, J., Shen, H., Russell, A.G., Nenes, A., Pappin, A.J., Napelenok, S.L., Bash, J.O., Fahey, K.M., Carmichael, G.R., Stanier, C.O., Chai, T., 2020. A multiphase CMAQ version 5.0 adjoint. Geosci. Model Dev. 13 (7), 2925–2944. https://doi.org/10.5194/gmd-13-2925-2020.

Zhuang, J., Jacob, D.J., Eastham, S.D., 2018. The importance of vertical resolution in the free troposphere for modeling intercontinental plumes. Atmos. Chem. Phys. 18 (8), 6039–6055. https://doi.org/10.5194/acp-18-6039-2018. https://acp.copernicus.org/articles/18/6039/2018/.